Heat partition in the $E/A = 8.5$ MeV $^{74}Ge + ^{165}Ho$ reaction

K. Kwiatkowski, R. Planeta,* S. H. Zhou,† and V. E. Viola
Department of Chemistry and Indiana University Cyclotron Facility, Indiana University, Bloomington, Indiana 47405

H. Breuer
Department of Physics, University of Maryland, College Park, Maryland 20742

M. A. McMahan
Accelerator and Fusion Research Division, Lawrence Berkeley Laboratory, Berkeley, California 94720

A. C. Mignerey
Department of Chemistry, University of Maryland, College Park, Maryland 20742
(Received 8 June 1989; revised manuscript received 5 September 1989)

The excitation-energy distribution of projectilelike fragments formed in the $E/A = 8.5$ MeV $^{74}Ge + ^{165}Ho$ reaction has been obtained by applying a statistical evaporation calculation to the difference between primary fragment mass yields derived from kinematic coincidence measurements and directly measured yields. A gradual transition from approximate equipartition of excitation energy for small energy losses to a division that favors the targetlike fragment for highly damped events is observed, in agreement with previous measurements. For a given energy loss, heat partition is found to correlate with the direction of net nucleon transfer. The variances of the excitation-energy distributions are shown to increase monotonically as a function of energy loss. The average data are compared with predictions of the nucleon exchange transport model. The results suggest that energy-loss mechanisms in addition to nucleon exchange may be important in the early stages of the collision.

I. INTRODUCTION

One of the most distinctive features of damped heavy-ion reactions is the rapid conversion of relative kinetic energy into heat during the lifetime of the dinuclear complex formed in the collision. For this reason, an experimental understanding of the thermal history of these short-lived systems as they evolve from nonequilibrated initial states towards full statistical equilibrium is central to any successful theoretical description of the process. Of particular interest in this regard is the question of how heat, or excitation energy, is partitioned between the reacting partners. Damped collisions at energies near or just above the barrier have been generally interpreted via transport models that account for energy dissipation in terms of nucleon exchange and/or particle-hole excitation between the projectile-like (PLF) and target-like (TLF) fragments.[1-5] In this context, statistical nucleon transfer between the fragments is the vehicle for heating of the system. For long interaction times the assumption of local equilibrium in the interacting zone should provide a satisfactory description of the thermalization process. However, in the early stages of the interaction, quantal[6-8] and/or collective[1-2,9-11] mechanisms may also come into play. These may subsequently exert an important influence on the evolution of the system toward equilibrium. Hence, measurement of the heat partition and associated fluctuations over a wide range of reaction times provides an important constraint on the theory of damped interactions.

Of practical concern, the nature of heat partition between the fragments at scission is essential to interpretation of the large body of inclusive nuclidic yield data that now exist for damped collisions. Direct comparison of experimental data with model calculations for charge and mass distributions is generally obscured by the decay of the highly excited primary fragments. Thus, significant corrections for light-particle evaporation must be applied to the measured data. These require a knowledge of how the heat/excitation energy is partitioned between the primary fragments, coupled with the application of a correction for statistical decay in order to translate the observed data into the primary distributions.

During the past decade a number of experiments and analyses have been performed which shed light on various aspects of excitation-energy sharing in damped collisions. Most of these studies have examined either a relatively narrow range of energy-damping associated with quasielastic events, or nearly symmetric target-projectile systems where the potential energy surfaces do not produce strong static driving forces for nucleon exchange. Several early experiments[12-17] suggested that full thermal equilibration might be achieved very early in the damping process, perhaps as low as $E_{loss} \simeq 50$ MeV. Equilibrium is indicated by an excitation-energy division ratio that corresponds to the mass ratio of the fragments.[12] However, subsequent work[18-22] has indicated that excitation energy is shared nearly equally between the reaction partners in the early stages of damping, but does not reach the full statistical equilibrium value, even

at very large energy losses ($E^* \simeq 150$ MeV). In addition, some of these studies have indicated that the partition of excitation energy is dependent on net nucleon exchange.[20,21,23]

In a recent paper[23] we investigated the $E/A = 9.0$ MeV $^{56}Fe + ^{165}Ho$ reaction in order to study the full range of energy damping for an asymmetric target-projectile combination. Both primary and secondary mass distributions were determined. The results confirmed that excitation energy is shared nearly equally for partially damped events and that the excitation-energy partition evolves gradually toward thermal equilibrium, approaching the mass ratio value only for fully damped events. These studies also permitted derivation of systematic estimates of the widths of excitation-energy distributions over a broad range of energy damping and also suggested that excitation-energy division depended on net nucleon transfer.

In this work we have studied the $E/A = 8.5$ MeV $^{74}Ge + ^{165}Ho$ reaction in order to study nucleon exchange in a heavier projectile-target system and to address the important question of the correlation between excitation-energy flow and net mass transfer. Relative to the $^{56}Fe + ^{165}Ho$ system, this system provides a greater range of energy damping; broader mass and charge distributions, which permit a more comprehensive investigation of the interrelationship between mass transfer and energy dissipation; minimal shell effects[24] in both target and projectile, and improved mass resolution for the primary fragments. Details of the nucleon-exchange character of the reaction are discussed in the preceding paper.[25] Here we focus on the conversion of relative kinetic energy of motion into internal heat for this system.

II. EXPERIMENTAL PROCEDURES

The details of the kinematic coincidence technique are contained in the companion paper[25] and in Ref. 23, which also describes the techniques whereby primary and post-evaporative mass distributions were determined. Here we describe the procedures used to translate the differences between the primary (A') and post-evaporative (A) masses, $\Delta A = A' - A$, into the excitation energy of the projectile-like fragment. Assuming a binary reaction mechanism (i.e., no preequilibrium particle emission), this then permits evaluation of the partition of excitation energy between the respective fragments.

In Fig. 1 logarithmic cross-section contours of the difference between primary and post-evaporative masses, ΔA, are plotted as a function of energy loss for projectile-like fragments. It is observed that the most probable ridge of the ΔA contours increases systematically with increasing energy loss. For very large energy losses, large mass loss and widths are observed, as expected for fission-like events. At low energy-loss values, where ΔA is small, the kinematic coincidence technique yields negative ΔA values for a fraction of the events due to finite mass resolution and recoil effects; e.g., for elastically scattered events, half of the values of ΔA must be less than zero due to finite mass resolution of the detection system. For this reason we restrict the energy-loss

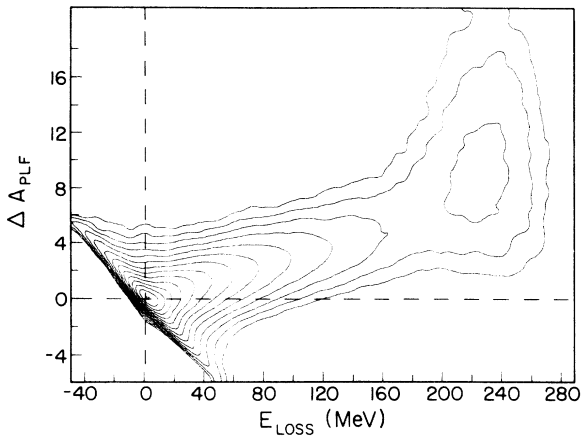

FIG. 1. Cross-section contours of evaporated mass, $\Delta A = A'_{\rm PLF} - A_{\rm PLF}$, as a function of energy loss for projectile-like fragments from the $E/A = 8.5$ MeV $^{74}Ge + ^{165}Ho$ reaction. The data have been smoothed in this plot for evaluating the average trends of the data. Contour lines are equally spaced on a logarithmic scale.

range to $E_{\rm loss} \geq 40$ MeV for the data presented in Sec. III, where the number of evaporated nucleons becomes statistically meaningful. In addition, Fig. 1 shows a correlation between $E_{\rm loss}$ and $\Delta A_{\rm PLF}$, visible as the diagonal distribution of the elastic-scattering cross section (along the 135° axis). This behavior is an artifact of the finite angular resolution of the TLF's, which are amplified by the large elastic-scattering cross section. These effects include intrinsic angular resolution in the multiwire proportional counter (MWPC), finite beam spot size, and scattering in the target and MWPC wire planes. These effects are most severe for elastic TLF recoils because of their low kinetic energies and unfavorable emission angle from the target.

Figure 2 gives the dependence of the centroids of the evaporative mass loss, $\langle \Delta A_{\rm PLF} \rangle$, as a function of primary fragment mass, A', for three representative energy-loss bins. To provide some perspective on the relative probabilities for different types of events, the size of the experimental points is made proportional to the logarithm of the relative yield. Two features should be noted in Fig. 2. First, the most probable evaporative mass loss becomes systematically larger for bins of increasing energy loss, as expected on the basis of the correspondingly larger excitation energies of the primary fragments. Second, for a given energy-loss bin, the evaporative mass loss increases as a function of increasing primary fragment mass.

To establish the correspondence between evaporated mass, ΔA, and excitation energy of the PLF, $E^*_{\rm PLF}$, iterative statistical-model calculations have been performed with the PACE-II code.[26] The program default values have been used and no discrete energy levels have been included. Input parameters were mass, charge, excitation energy, and spin of the PLF prior to evaporation. Atomic numbers from $Z = 15$ to 45 were included in the parameter space, each with 20 isotopes. The isotopic mass range was chosen in such a way that its centroid corre-

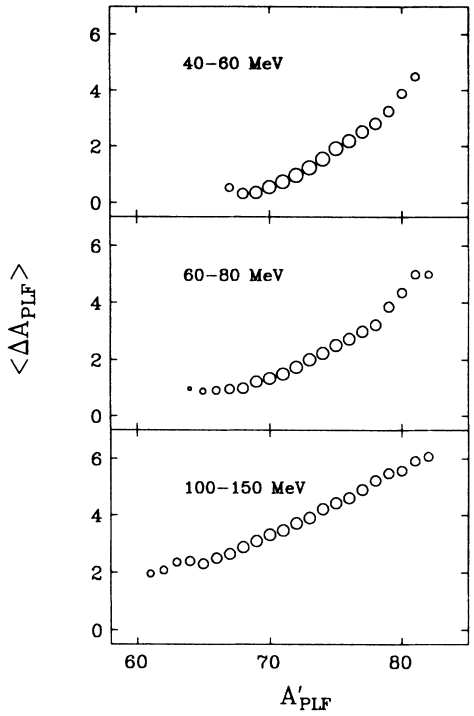

FIG. 2. Average evaporated mass versus primary fragment mass, A'_{PLF}, for representative energy-loss bins. The size of the points is proportional to logarithm of the cross section.

sponded to the most abundant primary mass for each element. The initial total excitation energy for each nucleus ranged from zero to 200 MeV; in the first 100 MeV, energy bins were split into 10-MeV segments and in the second 100 MeV the step size was 50 MeV.

The spin of the PLF was estimated using the total kinetic energy loss to parametrize the sum of the angular momenta of both fragments.[23] The range of angular momenta extended from the grazing limit for $E_{loss}=0$, $l_{max}=307\hbar$, to the fusion limit taken at $E_{loss}=240$ MeV, where $l_{fus}=115\hbar$, as taken from Wilcke *et al.*[27] A linear interpolation, dependent on E_{loss}, was taken between these limits. The same limits were used to calculate the fraction of the total angular momentum transferred to the PLF, i.e., zero transfer at the grazing limit and the value for classical sticking at the fusion limit.[28] The angular momentum distribution used in the PACE-II code was

$$P(l)=(2l+1)/(6l_{PLF}+1) , \quad (1)$$

where $l=l_{PLF}-1$, l_{PLF}, and $l_{PLF}+1$. The calculated values of PLF spin are found to be $L_{PLF}\simeq 6-10\hbar$ using this procedure. These are in general agreement with measured values.[29,30] Previous studies[23] have shown that for $L_{PLF}<15-20\hbar$ and $A_{PLF}>40$, the average number of evaporated nucleons is nearly independent of PLF spin. Thus, the results presented here are generally insensitive to assumptions concerning the PLF spin distributions.

The results of the evaporation calculations for the projectile-like fragments were tabulated as two functions:

$$f_{\Delta A}(A'_{PLF},Z'_{PLF},E^*_{PLF}):=A'_{PLF}-\langle A_{PLF}\rangle \quad (2)$$

and

$$f_{\Delta Z}(A'_{PLF},Z'_{PLF},E^*_{PLF}):=Z'_{PLF}-\langle Z_{PLF}\rangle , \quad (3)$$

where $\langle A_{PLF}\rangle$ and $\langle Z_{PLF}\rangle$ are the average calculated mass and charge centroids of the PLF after evaporation, respectively. Discontinuities caused by particle-emission threshold effects were smoothed by interpolating between the no evaporation limit at $E^*_{PLF}=0$ and the value of the calculation at $E^*_{PLF}=20$ MeV. An event-by-event iterative analysis was then performed on the results of Eqs. (2) and (3) to extract information about the excitation energy, E^*_{PLF}, and primary charge, Z'_{PLF}, for each event, using the measured values of Z_{PLF} and A_{PLF} and the reconstructed primary mass, A'_{PLF}. The steps in each iteration were as follows. First, the primary (preevaporative) charge was assumed to be $Z'_{PLF}(i-1)=Z_{PLF}+0.3$. The excitation energy for each iteration, i, was found by solving the equation for E^*_{PLF}:

$$f_{\Delta A}(A'_{PLF},\ Z'_{PLF}(i-1),\ E^*_{PLF}(i))=A'_{PLF}-A_{PLF} . \quad (4)$$

This can be solved unambiguously assuming that $f_{\Delta A}$ is a monotonic function of E^*_{PLF} for A'_{PLF} and Z'_{PLF}. Once the value of $E^*_{PLF}(i)$ is determined, it is then possible to calculate the quantity $\Delta Z_{PLF}(i)$, where

$$\Delta Z_{PLF}(i)=f_{\Delta Z}(A'_{PLF},\ Z'_{PLF}(i-1),\ E^*_{PLF}(i)) . \quad (5)$$

Convergence of the iteration was tested with a parameter,

$$\epsilon(i)=\Delta Z_{PLF}(i)-[Z'_{PLF}(i-1)-Z_{PLF}] . \quad (6)$$

If $|\epsilon(i)|<0.1$ charge units, the iteration was considered complete; if not, a new value of $Z'_{PLF}(i)$ was compiled from the function

$$Z'_{PLF}(i)=Z'_{PLF}(i-1)+0.9\epsilon(i) , \quad (7)$$

and the iteration was continued. The constant 0.9 was inserted to speed up the convergence. A maximum of 15 iterations was allowed, but most events converged in three steps or less. This procedure was applied only to events with $A'_{PLF}-A_{PLF}$ greater than zero.

Figure 3 shows the relationship between the average value of the evaporated mass, $\langle \Delta A_{PLF}\rangle$, as a function of energy loss and the average excitation energy derived from the event-by-event iterative procedure described in the preceding paragraph. The average behavior for all masses evolves as a nearly linear function of energy loss over the entire range of energy loss. Also shown in Fig. 3 is the same plot for selected mass bins equidistant below ($A'=68-70$) and above ($A'=78-80$) the projectile mass ($A=74$). As suggested by the results presented in Fig. 2, this analysis indicates that nucleon transfer from target to projectile leads to greater evaporative mass loss, and therefore higher than average excitation energies, or heating, of the PLF. Conversely, when the projectile transfers mass to the target, the results imply greater excitation-energy transfer and heating of the TLF. However, at least part of this dependence is due to experimen-

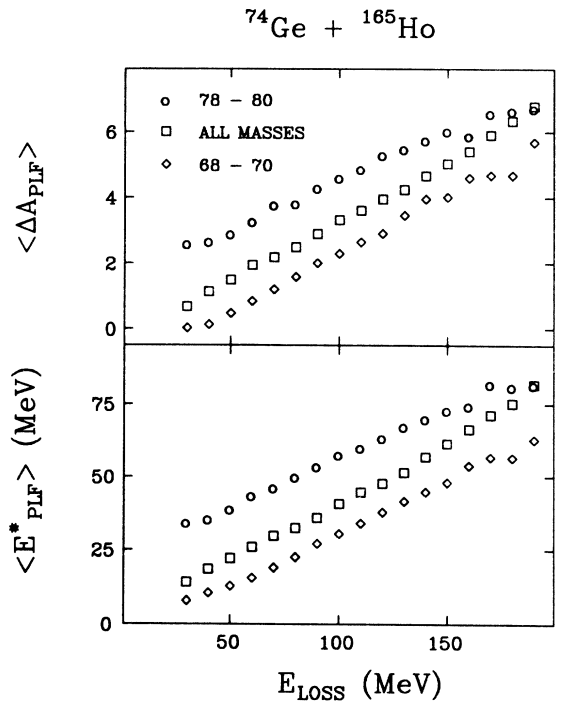

FIG. 3. (Top) Average evaporated mass as a function of energy loss. Squares represent the average over all masses; circles give results for primary masses, $A' = 78-80$, and diamonds are for primary masses $A' = 68-70$. (Bottom) Average PLF excitation energy derived from iterative statistical model fit to evaporated mass values, ΔA, in top curve. Symbols refer to the same mass bins as above.

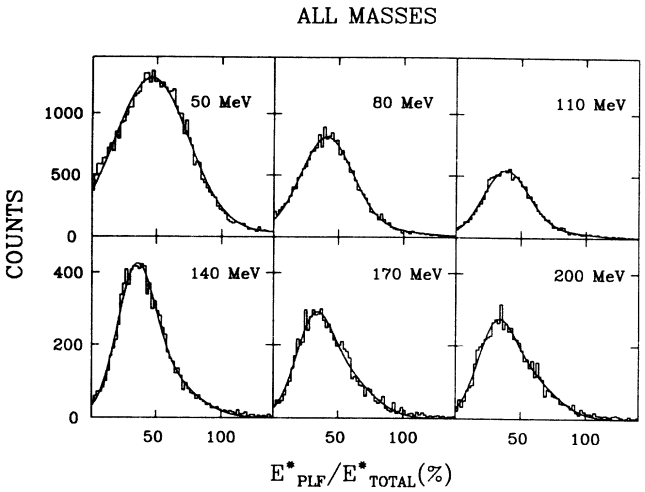

FIG. 4. Excitation-energy distributions for representative energy-loss bins (±5 MeV about centroid) as indicated on figure. Data are plotted in terms of percentage of PLF excitation energy relative to total available excitation energy. Solid lines represent fits to the data as described in the text.

tal correlations in the data.[31] This subject is investigated further in the Appendix.

Representative excitation energy spectra are shown in Fig. 4. Here we plot the distributions as a function of the *percentage* of the total available excitation energy, $(E^*_{\rm PLF}/E^*_{\rm total})\times 100$, for several energy-loss bins from 50 to 200 MeV. The solid lines represent an analytical fit to the data used to derive centroids and widths of the distributions. A Gaussian fit was applied for $E_{\rm loss} \leq 100$ MeV; for higher values a double Gaussian was applied in order to account for the skewed nature of the distribution. Centroids and widths were derived from the combined function. These data show the gradual decrease in the centroid of the fraction of excitation energy in the PLF as a function of increasing excitation energy. The widths remain similar for all $E_{\rm loss}$ bins. These results are discussed in greater detail in the following section.

It is noted that the distributions exhibit a finite probability at values of $E^*_{\rm PLF}/E^*_{\rm total} = 0$ and above 100%. This effect is associated with the experimental resolution of the system and the small values of $\Delta A_{\rm PLF}$ for partially damped events, which arise from recoil effects associated with nucleon evaporation and the finite mass resolution of the technique. For example, inspection of Fig. 3 (upper part) shows that for $E_{\rm loss} = 40$ MeV the mean value of ΔA is of the order of one. At this energy loss the primary mass resolution (FWHM) is approximately 1.2 u, whereas the secondary (measured) resolution is 0.6 u. The primary mass resolution was determined by a Monte Carlo simulation (see the Appendix). An *upper limit* for the elastic peak was found to be $\delta A' \leq 1.3$ u for the experimental data, assuming gates of $\delta E = 10$ MeV, $\delta A = 1$ u, and $\delta Z = 1$ unit [all full width at half maximum (FWHM)] on the secondary data for $A = 74$ and $Z = 32$. The finite mass resolution leads to a small fraction of events for which ΔA is negative. These systematic effects have been simulated by a Monte Carlo calculation and are included in the subsequent analysis and assignment of errors. It is estimated that these unphysical values of $E^*_{\rm PLF}/E^*_{\rm total}$ contribute errors of the order of 5% or less on the centroids of the distributions and 10% or less on the variances. All experimental values are summarized in Tables I, II, and III.

III. RESULTS AND DISCUSSION

Early investigations of fragment excitation-energy partition suggested that temperature equilibration in damped collisions might occur very rapidly, perhaps at energy losses as low as 50 MeV.[12–17] Simple Fermi gas arguments ($E^* = aT^2$) lead to the result

$$E^*_{\rm PLF}/E^*_{\rm tot} = A_{\rm PLF}T^2_{\rm PLF}/(A_{\rm TLF}T^2_{\rm TLF} + A_{\rm PLF}T^2_{\rm PLF}) , \quad (8)$$

where E^* is the excitation energy, T is the nuclear temperature and the level density parameter, a, is the same for both PLF and TLF. In the limit of equal fragment temperatures at scission, this relationship predicts excitation energy should divide according to the mass ratio $A_{\rm PLF}/A_{\rm tot}$. More recent studies have shown that at low-energy losses, the PLF receives more than its share of excitation energy up to energy losses well beyond 50 MeV.[18–23] In our previous $^{56}Fe + ^{165}Ho$ studies,[23] it was

TABLE I. Centroids and widths of excitation-energy distributions for the $E/A=8.5$ MeV $^{74}Ge+^{165}Ho$ reaction for data within ±5 MeV of stated energy loss. For the full-width-at-half-maximum value, Γ, the results for both the original data (Uncorr.) and the data corrected for experimental resolution (Corr.) are given. All masses are included.

E_{loss} (MeV)	$\langle E^*_{PLF}\rangle$ (MeV)	$\Gamma(E^*_{PLF})$ (MeV)		$\langle E^*_{PLF}/E^*_{tot}\rangle$ (%)	$\Gamma(E^*_{PLF}/E^*_{tot})$ (%)	
		Uncorr.	Corr.		Uncorr.	Corr.
40	18.5±0.14	35.5±0.9	24.2	52.3±0.4	76.5±2.8	55.6
50	22.1±0.20	40.7±1.7	30.7	49.1±0.4	70.7±2.7	50.4
60	25.9±0.57	42.0±3.5	31.5	47.2±0.6	65.3±4.6	45.4
70	29.6±0.44	46.6±2.7	36.3	43.9±0.5	64.5±6.7	46.7
80	32.4±0.55	49.2±3.1	38.2	43.2±0.8	59.9±6.3	42.3
90	35.8±0.86	51.3±4.2	39.1	42.2±0.8	58.5±7.4	42.2
100	40.6±0.87	54.5±4.7	41.1	42.1±0.9	56.0±5.8	40.3
110	44.5±0.88	60.5±5.0	46.5	42.5±1.5	55.0±8.2	40.2
120	47.6±1.1	61.8±7.3	45.2	41.8±1.5	53.2±8.1	38.8
130	51.4±1.9	67.0±9.7	48.9	41.8±1.6	53.0±9.0	39.4
140	56.8±1.5	71.4±8.1	51.1	42.2±1.5	53.6±8.8	40.7
150	61.4±1.9	78.8±10.6	57.1	41.7±1.8	52.1±9.7	39.1
160	66.5±1.7	85.9±8.5	62.3	42.5±1.8	54.0±9.6	41.8
170	71.3±1.9	87.2±11.1	58.9	43.3±1.6	55.3±8.4	43.4
180	75.2±2.4	91.2±12.7	58.7	42.9±1.9	55.3±10.8	43.1
190	81.5±2.2	94.7±12.8	56.8	43.6±1.7	53.8±9.4	40.6

TABLE II. Values of the average relative excitation energy in the projectile-like fragment, $\langle E^*_{PLF}/E^*_{tot}\rangle$ (in percent), as a function of energy-loss and primary fragment mass.

	E_{loss} (MeV)					
A'	40–60	60–80	80–100	100–150	150–200	200–250
54						25.4±1.0
55						25.3±1.4
56						24.7±2.0
57						24.4±3.0
58						29.4±2.6
59					31.4±2.9	27.8±1.5
60					31.4±2.7	31.1±0.95
61				24.5±1.3	30.7±2.2	27.5±0.99
62				25.1±0.96	28.0±2.0	29.1±0.81
63				27.6±1.0	28.7±1.6	31.1±1.4
64				32.0±0.64	32.8±0.99	32.8±1.0
65			23.7±1.9	27.9±0.64	32.0±1.3	33.5±2.0
66			27.9±1.0	30.1±0.48	33.9±1.2	34.0±1.4
67			24.7±1.3	30.7±0.53	35.3±0.89	35.6±1.1
68	31.1±1.1	26.2±1.9	29.6±0.62	33.1±0.72	34.0±1.5	33.7±1.2
69	21.6±1.6	30.7±1.0	30.5±0.57	34.7±0.52	35.2±0.99	36.4±1.3
70	34.9±0.56	34.0±0.41	34.7±0.39	36.4±0.53	36.2±0.92	35.6±1.2
71	29.3±0.79	33.6±0.47	35.6±0.38	36.7±0.51	37.3±0.86	35.2±1.3
72	38.0±0.89	35.8±0.35	36.8±0.35	38.3±0.54	37.7±0.98	35.1±0.92
73	37.2±0.46	39.7±0.34	39.1±0.35	39.8±0.57	38.3±1.1	36.3±1.1
74	47.6±0.30	44.6±0.29	42.4±0.32	42.1±0.58	40.1±1.3	35.4±0.99
75	53.8±0.46	48.8±0.30	46.1±0.66	43.5±0.62	39.8±1.1	35.0±1.0
76	57.4±0.32	52.2±0.44	48.8±1.0	45.3±0.75	41.2±1.0	37.5±1.0
77	63.2±1.1	56.3±0.83	52.0±1.4	47.7±0.72	43.2±1.1	37.0±1.1
78	65.3±1.2	58.5±0.72	55.2±2.4	50.0±0.65	43.4±1.6	40.0±1.2
79	69.6±1.9	63.9±1.7	57.9±2.8	52.4±1.0	43.5±1.9	40.1±0.99
80	78.4±3.9	69.9±2.3	61.4±2.0	52.4±1.2	46.2±1.2	42.1±1.0
81		85.1±3.4	60.7±4.2	55.3±2.0	49.3±2.1	42.8±0.90
82		86.3±3.9	65.4±2.6	54.9±2.8	48.9±1.5	43.0±1.0

TABLE III. Experimental full-width-at-half-maximum values (in MeV), $\Gamma(E^*_{PLF})$, and percentage of the width to the total available excitation energy, $\Gamma(E^*_{PLF}/E^*_{tot})$, as a function of primary fragment mass for three representative energy-loss bins.

	$\Gamma(E^*_{PLF})$			$\Gamma(E^*_{PLF}/E^*_{tot})$		
A' \ E_{loss}	40–60	60–80	100–150	40–60	60–80	100–150
61			39.0±16.6			38.7±10.9
62			33.6±6.9			37.0±6.7
63			45.3±8.1			42.8±9.2
64			38.2±6.5			41.0±4.8
65			48.1±7.0			41.7±4.2
66			46.6±6.5			41.3±3.6
67			50.3±4.1			46.8±3.3
68	26.4±3.8	31.9±3.4	48.3±4.7	61.4±9.2	57.0±9.8	48.1±4.7
69	32.3±2.8	33.4±2.9	48.2±4.0	74.5±6.8	56.5±6.6	43.8±3.3
70	27.0±1.4	30.7±5.4	43.1±3.4	62.7±3.5	50.3±2.5	42.6±3.5
71	32.1±1.4	34.7±2.0	46.6±4.8	75.0±4.0	57.3±2.7	42.9±3.6
72	30.7±1.2	33.1±2.5	48.8±4.6	62.7±5.4	53.2±2.3	43.0±3.7
73	32.3±1.1	33.5±2.7	50.5±5.5	71.5±2.3	52.7±2.2	45.8±4.2
74	28.9±1.1	33.2±4.3	49.2±6.7	61.9±2.0	48.9±2.2	43.1±4.3
75	28.0±1.6	33.8±4.8	48.8±6.1	58.0±3.2	48.0±2.3	44.0±4.6
76	32.5±2.2	34.4±4.4	50.5±7.5	63.4±2.3	49.6±3.3	44.2±5.7
77	31.6±4.6	33.6±5.6	53.2±6.4	58.9±8.1	50.7±6.2	44.4±5.1
78	30.6±4.3	37.7±5.1	52.2±5.8	57.6±9.4	50.1±5.5	44.5±4.7
79	34.3±6.2	35.4±4.8	58.5±9.3	60.2±16.3	47.7±14.7	47.1±8.4
80		40.8±13.6	60.1±9.6		59.1±16.6	48.8±9.6
81			60.3±11.1			48.8±14.8
82			63.0±12.0			51.9±22.0

demonstrated that energy equilibration is not a rapid process, but evolves gradually from equipartition of the energy in the quasielastic region to near the equal temperature limit for fully damped events. These studies provided systematic determinations of the widths of excitation-energy distributions over a broad range of energy loss and also suggested that the fragment receiving a net number of nucleons acquires more excitation energy per nucleon than its partner.

In this section we examine the dependence of the excitation-energy distributions for the $E/A = 8.5$ MeV $^{74}Ge + ^{165}Ho$ reaction on dissipated energy (E_{loss}) and net nucleon exchange. These results are compared with the predictions of models proposed to account for the experimental observables.

A. Excitation-energy partition

The average excitation-energy partition derived from the iterative statistical-model fits to the primary and post-evaporative fragment mass differences is first examined as a function of energy loss, E_{loss}. The centroids of the PLF excitation-energy distributions (Fig. 3 and Table I) show the expected increase in the internal excitation of the PLF as more energy is dissipated into the system. A more transparent representation of the partition of excitation energy is shown in the lower frame of Fig. 5, where the centroid of the ratio of PLF to total available excitation energy, $\langle E^*_{PLF}/E^*_{tot} \rangle$, weighted by cross section, is plotted. Also indicated on this plot are the corresponding ratios for equipartition of excitation energy and for

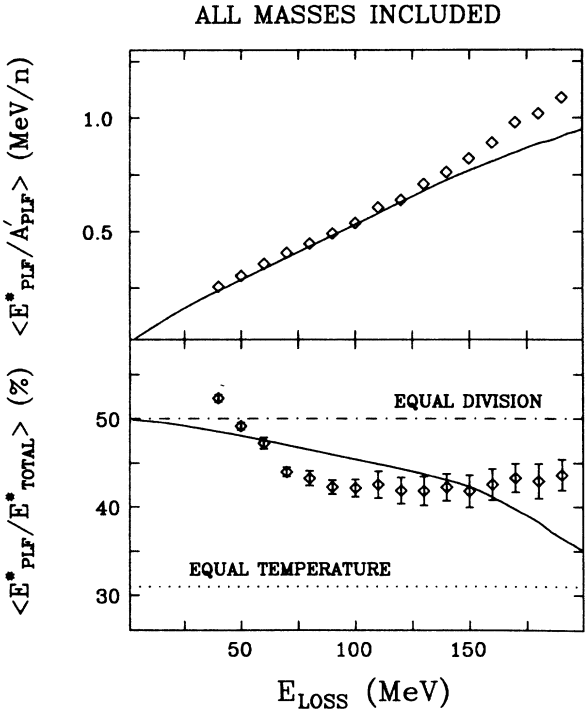

FIG. 5. (Top) Average of excitation energy divided by primary mass as a function of energy loss. Data are averaged over all masses. Solid line is the prediction of the nucleon exchange transport model in both figures. (Bottom) Average percentage of PLF excitation energy relative to total available excitation energy as a function of energy loss. Dot-dashed line indicates equipartition of excitation energy and dotted line is the equal temperature limit for a simple Fermi gas model, $A_P/A_{tot} = \frac{74}{239}$.

thermal equilibrium in a simple Fermi gas model with equal fragment level density parameters, i.e., $E^*_{PLF}/E^*_{tot} = A_{PLF}/A_{tot}$. Here we assume $A'_{PLF} = 74$ since $\langle A'_{PLF} \rangle$ decreases only slightly over this energy-loss range.

The experimental ratios exceed the equal energy-sharing ratio at energy-loss values below about 40 MeV and then gradually decrease at the amount of dissipated energy grows. For highly damped events, the average excitation-energy division ratio saturates at a value of about 0.41–0.44, which is considerably higher than the Fermi gas equal temperature value of 0.31. However, as will be discussed in the following, this result relates to the *average* event, and does not preclude the possibility that for some subset of events, the thermal equilibrium ratio can be achieved. Also noted in the lower part of Fig. 5 is a slight increase in $\langle E^*_{PLF}/E^*_{tot} \rangle$ at the largest E_{loss} values. This behavior is due to the increasingly skewed nature of the excitation-energy distributions at higher-energy losses (see, for example, Figs. 1 and 4). For the largest energy losses, the mass drift reverses direction and evolves toward symmetry as full damping is approached.[25] As will be shown in the following, the excitation energy of the light partner at fixed energy loss increases as a function of increasing fragment mass. Thus, as heavier PLF's (which include damped and/or fission products) assume increasing relative weight in the mass distribution, the average ratio of E^*_{PLF}/E^*_{tot} also increases.

The fundamental result of Fig. 5 is that thermal equilibration in damped collisions is not a sudden process, but evolves gradually on a time scale similar to that for nucleon exchange, energy damping and N/Z equilibration.[25] The solid line in the lower part of Fig. 5 and in Fig. 6 gives excitation-energy division ratios based upon the predictions of the nucleon exchange transport model[3] for this system. Here it is assumed[3] that $E^*_{PLF} = aT^2$, where T is the model prediction and $a = A/10$ MeV^{-1}. The model calculation assumes *a priori* that in the early stages of the collision, the exchange of a pair of nucleons leads to equal excitation of the reacting partners. Thereafter, the subsequent thermalization of the system is mediated by nucleon exchange. The model gives a qualitatively satisfactory description of the data except for quasielastic events. Similar predictions are obtained with the nucleon exchange transport model of Feldmeier[5] and the diabatic dissipative dynamics model of Nörenberg.[1,2]

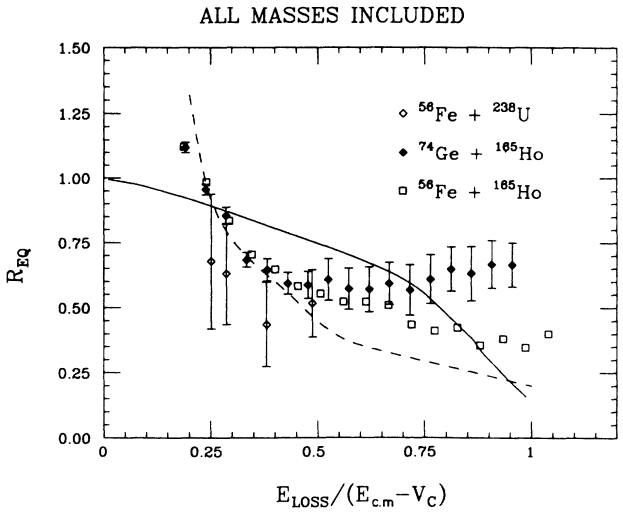

FIG. 6. R_{eq}, as defined by Eq. (9) as a function of energy loss divided by available energy above the Coulomb barrier. Data are from Ref. 19 (open diamonds), Ref. 23 (open squares) and this work (solid diamonds). Solid line is the prediction of the nucleon exchange transport model (Ref. 3) and dashed line is based on the random neck-rupture model (Ref. 32).

A more direct comparison of the data and the nucleon exchange transport model is provided in the upper frame of Fig. 5, where the ratio of the PLF excitation energy to primary mass, E^*_{PLF}/A'_{PLF}, is plotted versus E_{loss}. This quantity, which should be proportional to the square of the fragment temperature, exhibits nearly the same behavior as the model for energy losses below about 150 MeV.

In Fig. 6 we compare various data sets[19,23] for mass-asymmetric target-projectile systems that span a large range in E_{loss}. To normalize these three different target-projectile systems, we define a ratio, R_{eq}, given by

$$R_{eq} = \frac{\langle E^*_{PLF}/E^*_{tot} \rangle - A_P/(A_P + A_T)}{0.5 - A_P/(A_P + A_T)} , \tag{9}$$

where A_P and A_T are the mass numbers of the projectile and target, respectively. The numerator is defined in such a way that R_{eq} is one for equal excitation-energy division and vanishes for a division given by A_{PLF}/A_{tot}. The denominator serves to normalize the projectile-target mass asymmetry for the various data sets that span a large range of energy loss; specifically, $^{56}Fe + ^{238}U$ (Vandenbosch *et al.*, Ref. 19), $^{56}Fe + ^{165}Ho$ (Benton *et al.*, Ref. 23) and the present $^{74}Ge + ^{165}Ho$ system. In Fig. 6 we plot values of R_{eq} for these three systems as a function of the ratio of energy loss to available energy above the Coulomb barrier. Within the limitations of the experimental techniques and the normalization used to correlate the three systems, all these data sets appear to be self-consistent with one another.

Also shown in Fig. 6 is the predicted behavior for the R_{eq} parameter based on the nucleon exchange transport model (solid line) and the random neck rupture model of Brosa and Grossman (dashed line, calculated for the $^{56}Fe + ^{165}Ho$ system).[32] This model focuses on the final phase of separation, where a large fraction of the excitation energy may be stored as deformation energy in the neck between the fragments. During random rupture of the neck, the fragment that inherits the larger fraction of the neck obtains both excess mass and a disproportionately large fraction of excitation energy from the neck deformation energy. For the average quasielastic process, where there is little mass flow, this leads to equipartition of the energy. For fully damped events, which experience considerable nucleon flow from projectile to target, the TLF gains a larger share of the excitation energy. Both models reproduce the rough trends of the data.

In Fig. 7 the excitation-energy division ratio is shown for various primary mass bins. For large energy losses, one observes that the excitation energy partition is relatively independent of mass. However, with decreasing energy loss a dependence on PLF mass becomes apparent. Large transfers of mass from the PLF to TLF (low mass bins) lead to large amounts of excitation energy being transferred to the TLF and a relatively cold PLF; this $\langle E^*_{\rm PLF}/E^*_{\rm tot}\rangle$ ratio is nearly constant, just greater than the equal temperature value. For increasing mass bins, it is found that the relative amount of excitation energy in the PLF increases; i.e., the excitation energy appears to follow the direction of net mass transfer. Thus, if the PLF gains nucleons, it acquires more excitation energy than the average event; if the PLF loses nucleons, the TLF acquires excess excitation energy, in agreement with results from Refs. 20, 23, and 33.

This dependence of excitation-energy division on PLF mass and energy loss is tabulated in Table III. In Fig. 8 the excitation-energy ratio for PLF's is shown as a function of mass for six energy-loss bins ranging from partially damped events ($E_{\rm loss}=40$–60 MeV) up to the fully damped limit ($E_{\rm loss}=200$–250 MeV). Here one notes that for the smallest amount of damping ($E_{\rm loss}=40$–60 MeV), there appears to be a strong dependence of excitation-energy partition on PLF mass. With increasing damping this slope gradually flattens, until for complete damping it corresponds approximately to the equal-temperature value.

In all cases, the lightest observed fragments are found to be consistent with equal fragment temperatures. Detailed Monte Carlo simulations of these data have been carried out in order to examine instrumental correlations which also introduce mass-dependent correlations in the data (see the Appendix). These simulations indicate that the experimental technique and resolution effects—which are difficult to subtract from the data in a straightforward way—account for part of the observed effect. The major contribution to this instrumental correlation is associated with nucleon evaporation from the PLF recoils and the finite angular resolution for TLF's.

The dependence of $E^*_{\rm PLF}/E^*_{\rm tot}$ on the primary PLF mass for a given amount of energy dissipation is not addressed by current model calculations.[2,3,5] These experimental results combined with previous studies,[19–23] however, suggest that at least in the early stages of the reaction, factors in addition to statistical nucleon exchange associated with a one-body dissipation mechanism may exert an influence on the partition of excitation energy between the reacting partners.

Wilczyński[7] has pointed out that for asymmetric systems, the most peripheral interactions are dominated by proton transfer from projectile to target or neutron transfer in the reverse direction due to the corresponding asymmetries in the neutron and proton binding energies. This creates unequal neutron and proton fluxes which make the exchange of two like nucleons relatively unimportant for short interaction times. Siemens *et al.*[34] have

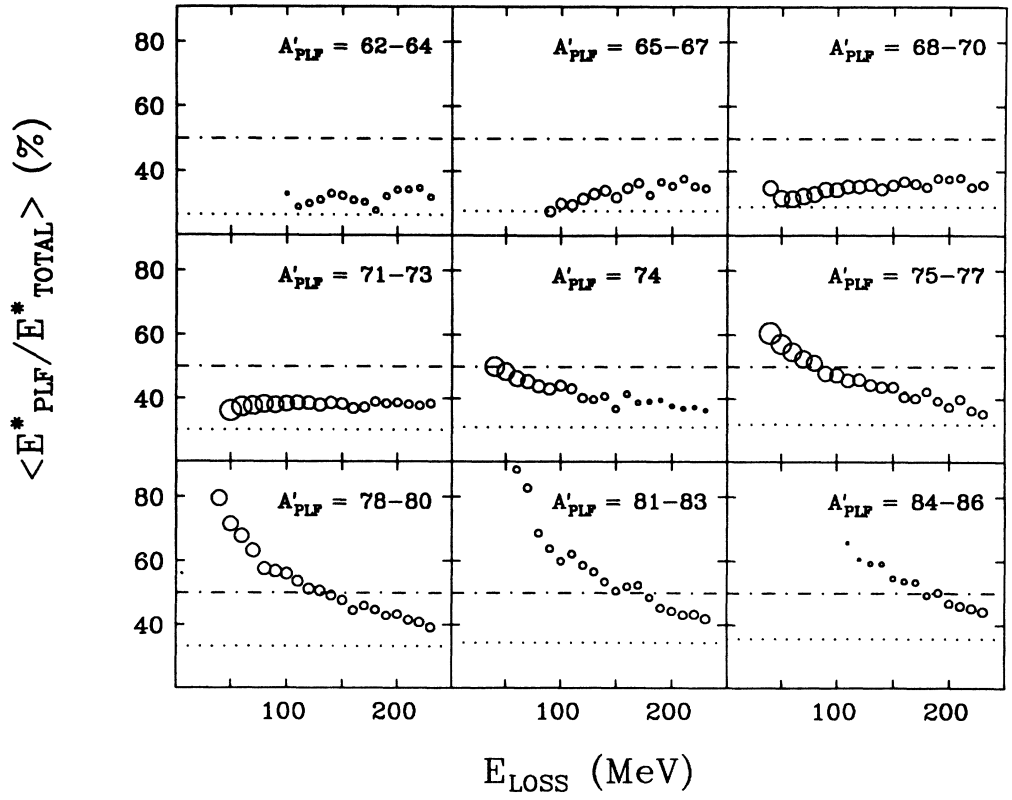

FIG. 7. Average of PLF excitation energy divided by total available excitation energy (in percent) as a function of energy loss for selected primary mass bins, as indicated on figure. Other symbols are as in Figs. 2 and 5.

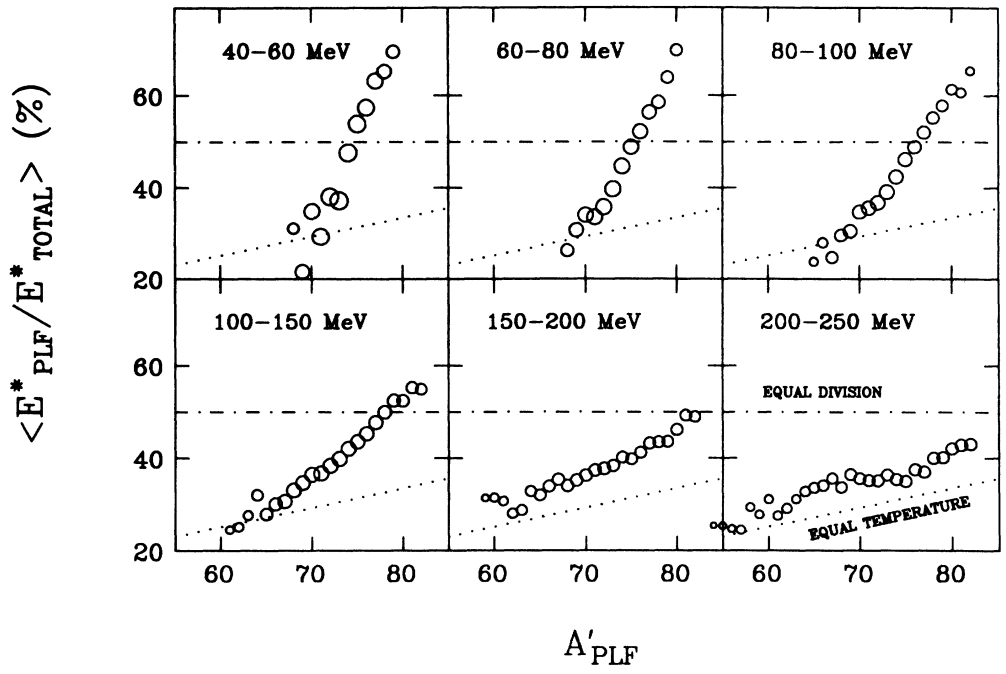

FIG. 8. Average of PLF excitation energy divided by total available excitation energy (in percent) as a function of primary PLF mass for several energy-loss cuts. Symbols are the same as Figs. 2 and 5.

pointed out that this situation creates a thermal mismatch between the reacting partners, which must subsequently affect the statistical evolution of the system at smaller interaction distances and longer times. In addition, the possible contributions of other energy dissipation mechanisms such as the excitation of giant resonances[11] and charge exchange[8] cannot be overlooked.

Attempts to address the quantal aspects associated with the early stages of damped collisions—which provide a basis for explaining the correlation between net nucleon flow and excitation-energy partition—have been addressed by Nörenberg[1,2] and Griffin.[6] Nörenberg and co-workers[1,2] have considered the combined effects of coherent coupling between collective and intrinsic degrees of freedom and the subsequent equilibration of the system by residual two-body collisions. In this model, a diabatic two-center shell model is used to account for fragment excitation via particle-hole excitations. Griffin and Broniowski[6] have employed a Schrödinger double-shell model to show that Schrödinger dynamical flow, driven by kinetic pressures, does not necessarily conform to nucleon exchange models, especially in the early stages of the interaction. Qualitative intercomparison of these approaches is not possible at present, but their success in accounting for the dependence of heat partition on net nucleon exchange should provide an important test of their applicability.

The feedback mechanism of Moretto and Lanza[9] and Schmidt[10] provides an attractive qualitative explanation of the association between excitation energy flow and net nucleon exchange. This model has the complementary advantage of providing a mechanism for explaining the deviation[25] between the direction of nucleon flow as observed in the experimental data and that predicted by the nucleon exchange transport model. The basic premise of the model is that the initial transfer of one or more nucleons leads to a higher temperature for the acceptor nucleus (see also Ref. 34). For example, nucleon exchange, which leads to equal excitation of both partners ($E^*_{\rm PLF}=E^*_{\rm TLF}$), will lead to a higher temperature in the light partner since $E^*/A_{\rm PLF} > E^*_{\rm TLF}/A_{\rm TLF}$. This creates a thermal driving force which competes with the static and dynamical forces associated with the statistical exchange of nucleons. This temperature mismatch leads to the subsequent transfer of nucleons in the opposite direction in order to raise the temperature of the cooler (TLF) fragment. For asymmetric collisions between very heavy ions such as those discussed here, Q-value considerations favor the initial transfer of a neutron from target to projectile. This effect is experimentally observed in the nuclide distributions for low-energy losses.[20,23,35] Thus, on the average the projectile-like partner acquires a disproportionate share of the initial excitation energy, leading to $E^*_{\rm PLF}/A'_{\rm PLF} > E^*_{\rm TKF}/A'_{\rm TLF}$, or $T_{\rm PLF} > T_{\rm TLF}$.

In this context, the subsequent evolution toward thermal equilibrium is more efficiently achieved by excitation of the TLF via transfer of nucleons from projectile to target, rather than by the exchange of nucleon pairs. The importance of this effect may be coupled to the gradient in the relevant potential energy surface, as pointed out by Błocki;[36] weak gradients serve to enhance thermal feedback. At the same time, attainment of N/Z equilibration favors the transfer of protons from PLF to TLF. This argument should be most relevant for short interaction times where the net number of nucleon transfers ($\Delta A_{\rm PLF}$) is large with respect to the total number of nucleon exchanges, as deduced from experimental variances of the mass distributions.[25] As the interaction time in-

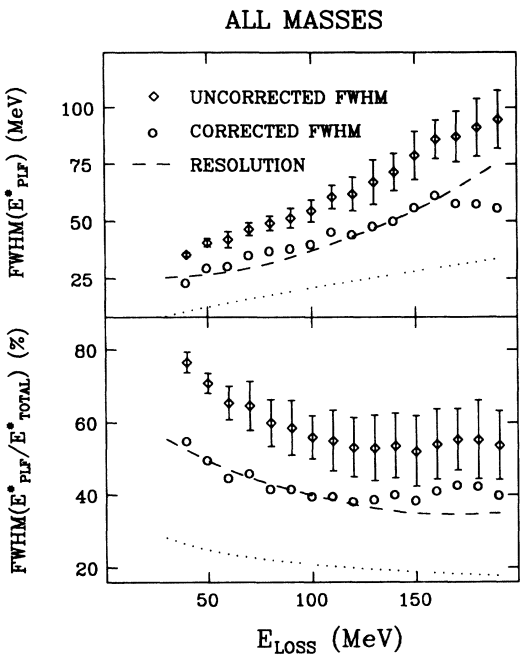

FIG. 9. (Top) Full width at half maximum of excitation energy distribution as a function of energy loss. Data are averaged over all PLF primary masses. Diamonds present raw data; dashed line is the calculated resolution of the system, and circles are resolution-corrected final data. For both figures, the dotted line is the prediction for fragments in thermal equilibrium (Ref. 37). (Bottom) Percentage of PLF excitation-energy width to total available excitation energy as a function of energy loss.

creases, the development of statistical exchange should grow in importance, leading to eventual thermalization of the system for which $T_{PLF} = T_{TLF}$, or $E^*_{TLF} \simeq (A'_{TLF}/A'_{PLF})E^*_{PLF}$. Thus, inclusion of the thermal feedback effect provides a useful mechanism for interpreting the observed correlation between net nucleon transfer and excitation energy partition between the fragments, as has been previously discussed in Ref. 23.

In concluding this section it should be remarked that *for the average event,* where the net transfer of nucleons is small, the excitation-energy partition is in general agreement with the nucleon exchange-transport model.[3] It is only in the wings of the primary mass distributions at fixed energy loss—where the model does not make any predictions—that the correlation between mass transfer and excitation energy becomes most apparent.

B. Excitation-energy distribution widths

In addition to the average heat partition properties associated with net nucleon transfer and energy dissipation, the width of the excitation distribution, $\Gamma(E^*)$, is an equally important reaction parameter. Here we define $\Gamma(E^*)$ as the full width at half maximum, as derived from distributions such as those shown in Fig. 4. Due to experimental resolution and uncertainties associated with broadening effects from particle evaporation from the reaction partners, absolute width information is subject to greater error than for centroids of the distributions. For this reason, resolution corrections were estimated via Monte Carlo calculations and these have been subtracted in quadrature from the experimentally derived width data presented in Figs. 9 and 10 and Table III. The correc-

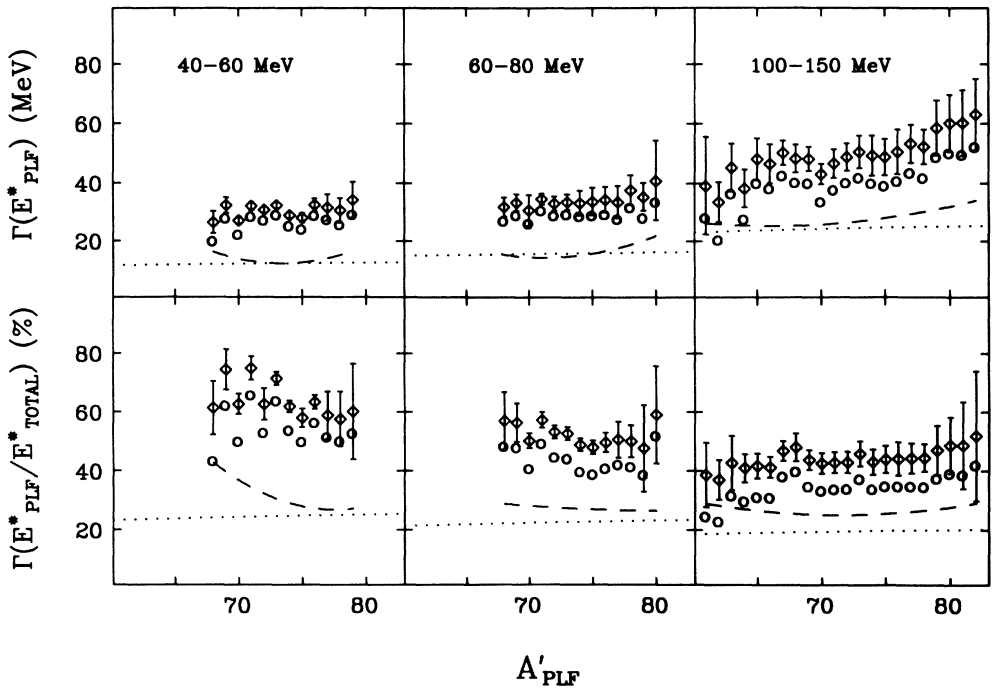

FIG. 10. (Top) Full width at half maximum of excitation-energy distribution as a function of PLF primary mass for representative energy-loss bins. All symbols are the same as Fig. 9. (Bottom) Percentage of PLF excitation-energy width to total excitation energy as a function of PLF primary mass.

tions include contributions from evaporation recoil effects, PLF and TLF detector angular resolution, PLF detector mass resolution and PLF kinetic energy resolution. The resolution calculations are indicated by a dashed line in Figs. 9 and 10; diamonds refer to the experimental data and circles are the resolution-corrected widths in these figures. These values are given in Table I and Table III.

In Fig. 9 the dependence of the absolute width, $\Gamma(E^*_{\rm PLE})$, on energy loss is shown in the upper frame and the width of the excitation-energy distribution relative to the total available excitation energy, $\Gamma(E^*_{\rm PLF}/E^*_{\rm tot})$, is shown in the lower frame. These values represent a superposition of many individual widths for the measured nuclide distribution and thus are greater than those shown for individual masses (Fig. 10). The absolute corrected widths increase monotonically as a function of increasing total excitation energy of the system (or $E_{\rm loss}$). One observes that the widths are relatively broad; this has important implications for any attempts to relate inclusive yield distributions to primary values, since it significantly broadens the number of species that can be derived from a given total excitation energy. The ratio of the PLF width to the total excitation energy is found to remain relatively constant as a function of increasing energy loss, except for events in the quasielastic region. Both representations of the widths demonstrate that the thermal fluctuations are large in these reactions. At present no theoretical predictions from the nucleon-exchange-transport models[3-5] or the dissipative diabatic dynamics model[1,2] exist with which to compare these results. The absolute corrected widths are qualitatively similar to those reported previously for the ^{56}Fe+^{165}Ho system;[23] however, our values at high $E_{\rm loss}$ are about 25 percent lower due to larger resolution corrections determined in the current work. On the other hand, the dependence of the fractional widths on $E_{\rm loss}$ is nearly identical for both systems.

In Fig. 10 and Table III values of $\Gamma(E^*_{\rm PLF})$ and $\Gamma(E^*_{\rm PLF}/E^*_{\rm tot})$ are presented as a function of primary fragment mass for several energy-loss bins. Within experimental uncertainties neither the absolute nor the fractional corrected widths exhibit any appreciable dependence on PLF mass number, although for the 100–150-MeV bin there appears to be a systematic increase in the absolute width with increasing mass. Again, these results are in agreement with the data of Ref. 23 for the ^{56}Fe+^{165}Ho system.

The dotted lines in Figs. 9 and 10 are derived from the model of Morrissey and Moretto[37] for the excitation-energy widths of a system with equal temperature at scission and the assumption of a Gaussian excitation-energy distribution. The calculations assume a level density parameter $a = A/8$ MeV^{-1}. This prediction reproduces the qualitative trend, but underestimates the absolute magnitude of the data by about a factor of 2. Since the calculation assumes thermal equilibrium, the observed disagreement is not surprising. Nonetheless, the comparison is valuable in highlighting the larger fluctuations associated with nonequilibrated systems as they evolve toward thermal equilibrium.

IV. CONCLUSIONS

Examination of the excitation-energy distributions for the $E/A = 8.5$ MeV ^{74}Ge+^{165}Ho reaction have reinforced and amplified the conclusions of previous investigations of heat partition in damped collisions.[18-23] These studies, performed with improved PLF nuclide resolution, provide heat partition data over nearly the full range of energy damping for an asymmetric projectile-target system with minimal shell effects.

The average behavior of the PLF excitation energy relative to the total available excitation energy decreases from values slightly greater than for equipartition of energy at small energy losses to values that favor excess excitation energy in the TLF for fully damped events (Fig. 5). General agreement is found with the average values calculated with the nucleon exchange transport model.[3] However, for partially damped events the excitation-energy sharing favors the PLF, rather than equal sharing as would be expected for the exchange of a pair of nucleons. This behavior is consistent with more detailed studies of this energy-loss region in other systems.[20]

The data indicate a correlation between net nucleon transfer and the heating of the acceptor nucleus (Figs. 7 and 8). That is, fragments which gain nucleons during the projectile-target interaction time acquire a disproportionate share of the excitation energy. This correlation appears to be most important for small values of energy loss, or short interaction times. With increasing energy damping, the dependence of the heat partition on net nucleon transfer becomes gradually weaker until, for fusion-fission like events, it approaches the thermal equilibrium limit, $E^*_{\rm PLF}/A_{\rm PLF} = E^*_{\rm tot}/A_{\rm tot}$. These results suggest that mechanisms other than the statistical exchange of nucleon pairs may play an important role in thermalization of the dinuclear complex, particularly in the early stages of the reaction.[1,2,6-11] The thermal feedback model,[9,10] which emphasizes the role of nucleon transfer in the initial heating of the system, provides a useful mechanism for examining the competition between the drive toward thermal equilibrium and the static and dynamic forces imposed by the statistical transport properties of the system. It remains an important test of theoretical models of damped collisions to explain this behavior satisfactorily.

The widths of the excitation-energy distributions are found to be generally broad, even for relatively low-energy losses, and increase systematically with increasing total excitation energy (Figs. 9 and 10). The ratio of the PLF width to the total available excitation energy, however, is rather insensitive to either the amount of energy dissipated in the collision or the net mass transfer for a specific energy loss. Comparison of the experimental widths with predictions based on a dinuclear system in thermal equilibrium[37] demonstrates that the experimental values are significantly larger than calculated. This result emphasizes the nonequilibrium nature of these systems.

The implications of these results for exotic nuclide synthesis via damped collisions should also be noted. The observed dependence of excitation energy on net nucleon

transfer indicates that on the average fragments that have gained a large number of nucleons will be highly excited, and thus more susceptible to particle decay. For this reason, neutron-excess isotopes of PLF's with $Z>Z_{proj}$ and TLF's with $Z>Z_{tar}$—the primary objects of such studies—will be affected most severely by depopulation due to particle decay. One compensating factor, however, is that the widths of the excitation-energy distributions appear to be sufficiently broad that a finite probability exists for forming exotic species in a relatively cold state.

In summary, these results demonstrate that the heat partition properties associated with the damped collisions at near-barrier energies provide a new dimension for the theoretical investigation of these processes. The importance of nucleon transfer in the conversion of relative energy of motion into internal heating of the system is suggested by these data and indicates the need for incorporation of this additional degree of freedom into the full transport model calculations.

ACKNOWLEDGMENTS

The authors wish to thank R. Vandenbosch, J. Wilczyński, and J. Randrup for valuable discussions concerning this work. In addition, we are also grateful to J. Randrup for making his nucleon exchange transport model code available to us. We acknowledge the valuable discussions of J. Toke, W. U. Schröder, and J. R. Huizenga concerning the problem of instrumental correlations in the data analysis. We appreciate the assistance of K. Morley with some of the Monte Carlo simulations associated with this work. This research was supported by the U. S. Department of Energy and the National Science Foundation.

APPENDIX

Because the coincidence data described in this paper involve (1) a large number of experimental parameters and (2) the use of statistical models to obtain the final results, we have performed detailed Monte Carlo simulations to investigate the sensitivity of the data on the technique and associated instrumental effects. Here the quantity δ represents the experimental FWHM value. The input parameters for these simulations were: (1) the laboratory kinetic energy, mass, and charge of the ^{74}Ge projectile; (2) the mass and charge of the ^{165}Ho target; (3) position and angular acceptance of the PLF detector (26.5°, $\Delta\theta=1.2°$); (4) angular resolution of the PLF ($\delta=0.1°$) and TLF detectors. The TLF resolution was based on measured angular correlations for elastic TLF's, with gates set on elastic PLF's with $\delta=6$ MeV and the values listed in (5); this is a worst-case assumption because elastic TLF's are the most poorly resolved in our system due to their low energies and unfavorable emission angle from the target. (5) experimental mass ($\delta=0.6$ u) and charge ($\delta=0.6$) resolution of the PLF detector telescope; (6) parameters a', b', and k of a two-dimensional Gaussian parameterization[38] of the primary fragment cross-section distribution in the N-Z plane for the projectile-like fragments (to be found in Ref. 25); (7) the total kinetic energy loss, E_{loss}, and (8) a functional dependence of the excitation-energy division ratio, E^*_{PLF}/E^*_{tot}, on PLF primary mass and energy loss, where the PLF excitation energy and the total excitation energy E^*_{tot} were given by

$$E^*_{tot}=E_{loss}+Q_{gg}(A'_{PLF},Z'_{PLF}) . \tag{10}$$

In our calculation Q_{gg} was approximated by the liquid-drop model mass formula.[39]

In the first step the simulations generated the primary mass and charge of the PLF from a two-dimensional Gaussian distribution with parameters described in Refs. 38 and 40. The initial direction of the fragments was determined by an assumed c.m. angular distribution ($d\sigma/d\Omega\simeq 1/\sin\theta_{c.m.}$). Other shapes of the angular distribution function were also examined; for our system this effect was found to be rather unimportant because of the small angular acceptance of the PLF detector. In the next step, velocities of the two primary reaction products in the c.m. system were calculated.

The post-evaporation PLF mass and charge were generated according to the prediction of the statistical code PACE-II for a given E^*_{PLF} and angular momentum window, as discussed in Refs. 10 and 23.

Evaporated mass from the TLF was approximated by the formula

$$\Delta A_{TLF}=\Delta A_{PLF}(E^*_{TLF}/E^*_{PLF}) . \tag{11}$$

One can also use the approximation $\Delta A_{TLF}=E^*_{TLF}/12$ with equal success. The light-particle evaporation recoil effect was simulated by a Maxwellian distribution[41] given by

$$d^2\sigma/d\Omega dv_R=v_R^2\exp(-v_R^2/2s_i^2) , \tag{12}$$

where

$$s_i^2=\Delta A_i T_i/(A'_i-\Delta A_i)^2; i=\text{PLF,TLF} . \tag{13}$$

Here A'_i and ΔA_i correspond to the primary mass and the evaporated mass for PLF and TLF, respectively; T_i was the corresponding temperature of the fragment and the average neutron evaporation energy was taken to be $1.5\,T_i$.

The final velocity of a fragment was given by

$$\mathbf{v}_i=\mathbf{v}_0+\mathbf{v}'_{i,c.m.}+\mathbf{v}_{i,R},\quad i=\text{PLF,TLF} . \tag{14}$$

Here $\mathbf{v}_0$ was the velocity of the composite system and $\mathbf{v}'_{i,c.m.}$ denoted the initial center-of-mass velocity of each primary fragment. The $\mathbf{v}_{i,R}$ represented the recoil velocity.

To take into account the finite mass and charge resolution of the detected PLF, we randomized these quantities to achieve the measured values. A similar randomization procedure was applied to the PLF and TLF final direction.

Only those events were selected for which the PLF falls into the acceptance window of the corresponding detector. For each accepted event the following quantities were generated: (1) for the secondary PLF: A_{PLF}, Z_{PLF}, E_{PLF}, θ_{PLF}, ϕ_{PLF}, and (2) for the corresponding TLF:

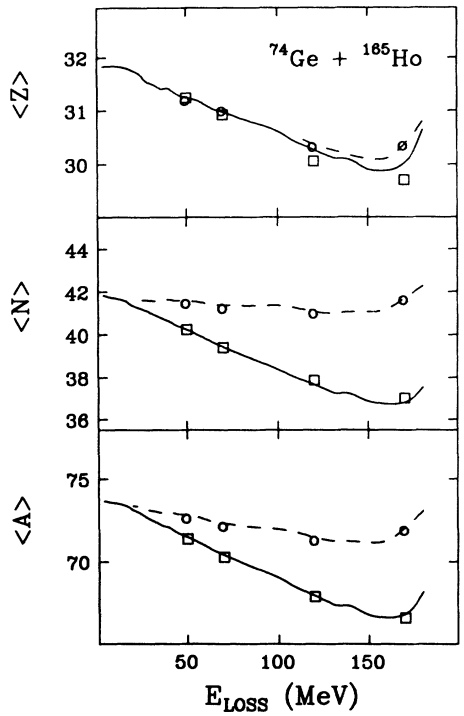

FIG. 11. Centroids of the PLF proton (top), neutron (center), and mass (bottom) number distributions as a function of energy loss. Monte Carlo simulations described in the Appendix are indicated by squares for the experimental data and circles for the primary distributions. Solid lines represent the measured experimental centroids, and dashed lines refer to the primary centroids.

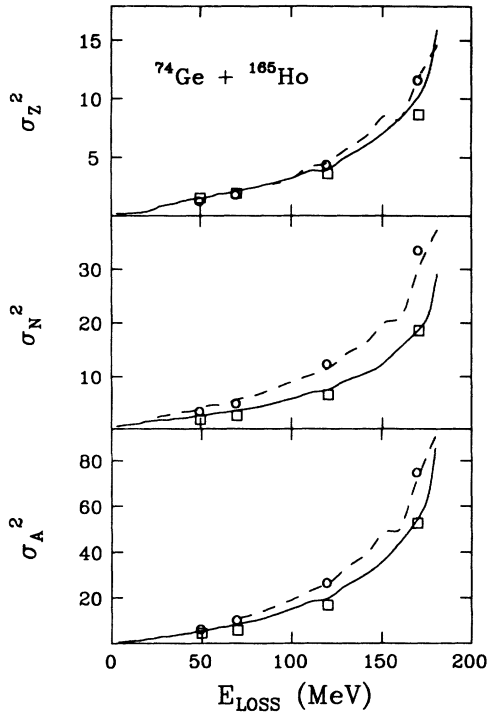

FIG. 12. Variances for proton (top), neutron (center), and mass (bottom) number distributions. Symbols are same as in Fig. 11.

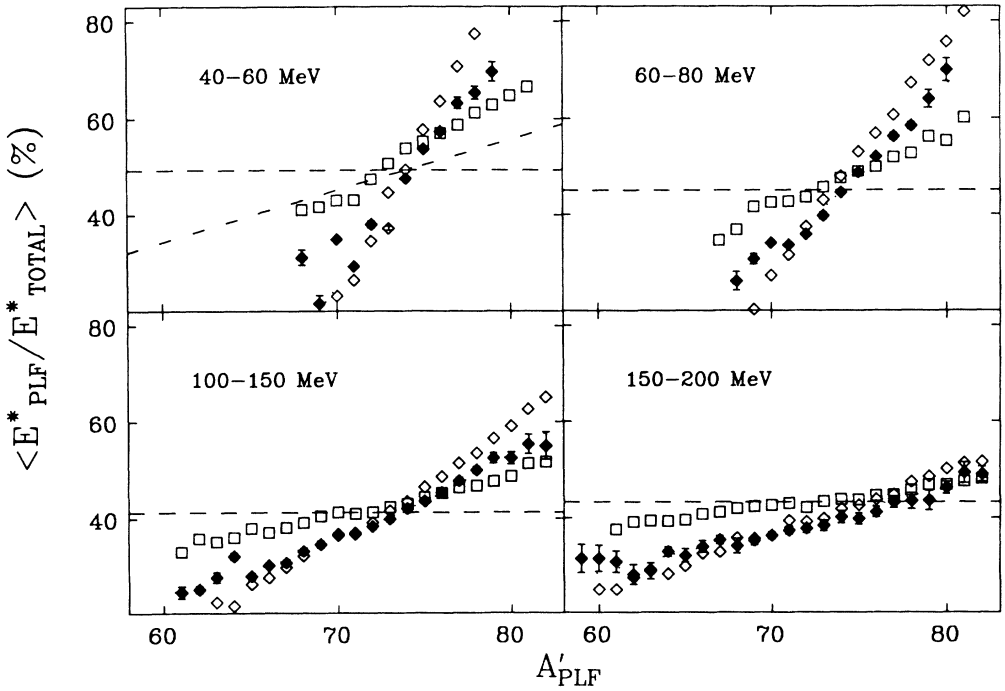

FIG. 13. Average ratio of PLF excitation energy to total available excitation energy in percent. Experimental data are given by solid diamonds. Open diamonds represent Monte Carlo simulations described in the Appendix, assuming the average behavior of the experimental data (dotted line). Open squares are Monte Carlo simulations assuming the average value of excitation-energy partition predicted by the nucleon exchange transport model (Ref. 3), independent of mass (dashed line). Dotted-dashed line is based on the analytical formula of Ref. 31, assuming independence of excitation energy division on fragment mass.

θ_{TLF}, ϕ_{TLF}.

This set of physical parameters was identical to that extracted from the experimental data.[25] We subsequently analyzed these simulated "data" in the same way as the measured ones. As a result, we obtained information about the primary mass, charge, kinetic energy, and excitation energy of the PLF. In addition to mean values of these quantities, we obtained information about the corresponding widths due to the experimental technique.

Figs. 11 and 12 show that the simulations reproduce the measured centroids and variances of the Z, N, and A distributions quite well. These calculations use the experimentally determined excitation-energy division ratios (summarized by the dotted lines in Fig. 13). Here the solid line represents the experimental (post-evaporative) data and the dashed lines the primary fragment centroids. The squares and circles show the simulation results at representative energy-loss values for the post-evaporative and primary centroids, respectively.

Figure 13 compares the data (solid points) for representative energy-loss bins from Fig. 8 with Monte Carlo simulations involving two quite different assumptions about the dependence of excitation-energy partition on PLF mass. First, the open diamonds show results that assume a mass-dependent value for E^*_{PLF}/E^*_{tot} as a function of primary mass for a given energy-loss bin. (The average behavior of the experimental data used in the simulation is given by the dotted line.) As a second assumption (open squares) it is assumed that E^*_{PLF}/E^*_{tot} is independent of fragment mass and given by the average value of the experimental data (dashed line). Also shown is the prediction (dot-dashed curve) of an analytic formula derived by Töke *et al.*,[31] which predicts the experimental resolution contributions to the dependence of excitation-energy division on primary mass. This formula requires a knowledge of the primary mass distribution. It is observed that the technique and instrumental effects introduce a dependence of E^*_{PLF}/E^*_{tot} on PLF mass. Subtraction of this effect from the data is not straightforward and thus we choose to compare the experimental and simulated results directly in Fig. 13. A more direct comparison is shown in Fig. 14, where the simulations are compared with the data for the evaporated mass, ΔA_{PLE}, as a function of the primary fragment mass for the two widely separated energy-loss bins. As before, the open diamonds represent simulations that assume the average dependence of the energy loss on PLF primary mass, as deduced from the data (dotted line in Fig. 13); the open squares assume that for a given energy loss, excitation-energy partition is independent of fragment mass. Here the mass-independent assumption for the E^*_{PLF}/E^*_{tot} at fixed E_{loss} is clearly in disagreement with the data.

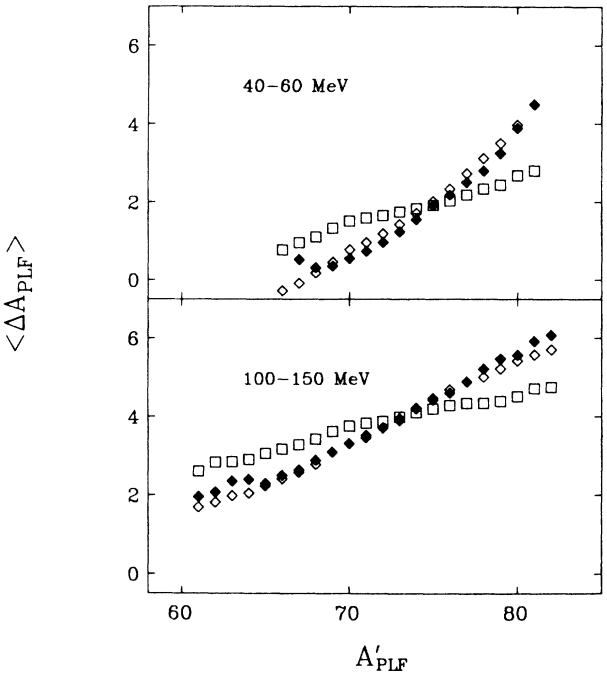

FIG. 14. Average PLF evaporated mass as a function of primary fragment mass for two energy-loss bins, as indicated on figure. Solid diamonds are experimental results of Fig. 2. Open diamonds are Monte Carlo simulations assuming the experimental excitation-energy division values. Open squares indicate results which assume excitation-energy division is independent of mass.

In summary, Monte Carlo simulations that include all known resolution effects and physics parameters of the method are found to reproduce these data satisfactorily. Recoil effects due to light-particle evaporation and TLF angular resolution are found to account for the major sources of uncertainty. This introduces a dependence of the excitation-energy partition at fixed E_{loss} on fragment mass. However, the magnitude of this effect is below that observed experimentally.

*Permanent address: Institute of Physics, Jagellonian University, Reymonta 4, 30-059 Kraków, Poland.

†Permanent address: Institute of Atomic Energy, Beijing, People's Republic of China.

[1]W. Nörenberg, *New Vistas in Nuclear Physics*, edited by P. J. Brussard and J. H. Koch (Plenum, New York, 1986), p. 81.

[2]Z. He, P. Rozmej, J. Wu, and W. Nörenberg, Nucl. Phys. **A473**, 342 (1987).

[3]J. Randrup, Nucl. Phys. **A307**, 319 (1978); **A327**, 490 (1979); **A303**, 468 (1982).

[4]W. U. Schröder, R. T. DeSouza, J. R. Huizenga, and L. M. Schneider, *Proceedings of the International Symposium on Nuclear Fission and Heavy-Ion-Induced Reactions, Rochester, 1986* (Harwood Acedemic, New York, 1987), p. 255.

[5]H. Feldmeier, Rep. Prog. Phys. **50**, 1 (1987).

[6]J. J. Griffin and W. Broniowski, Conference on Theoretical Approaches of Heavy-Ion Reaction Mechanisms, Paris, 1984, University of Maryland Report ORD-5126-218, 1984.

[7]J. Wilczyński and H. W. Wilschutt, Phys. Rev. C **39**, 2475 (1989).

[8]H. Hoffman, C. Grégoire, R. Lucas, and C. Ngô, Z. Phys. A **293**, 229 (1979).
[9]L. G. Moretto and E. G. Lanza, Nucl. Phys. A **428**, 137c (1984).
[10]R. Schmidt, Nucl. Phys. **A445**, 534 (1985).
[11]R. Broglia, C. H. Dasso, and A. Winther, Phys. Lett. **53B**, 301 (1974).
[12]D. Hilscher, J. R. Birkelund, A. D. Hoover, W. U. Schröder, W. W.Wilcke, J. R. Huizenga, A. C. Mignerey, K. L. Wolf, H. F. Breuer, and V. E. Viola, Jr., Phys. Rev. C **20**, 576 (1979).
[13]R. Babinet, B. Cauvin, J. Girard, H. Nifenecker, B. Gatty, D. Guerreau, M. Lefort, and X. Tarrago, Nucl. Phys. **A296**, 160 (1978).
[14]B. Cauvin, R. C. Jared, P. Russo, R. P. Schmitt, R. Babinet, and L. G. Moretto, Nucl. Phys. **A301**, 511 (1978).
[15]Y. Eyal, A. Gavron, I. Tserruya, A. Fraenkel, Y. Eisen, S. Wald, R. Bass, C. R. Gould, G. Kreyling, R. Renfordt, K. Stelzer, R. Zitmann, A. Gobbi, U. Lynen, H. Stelzer, I. Rode, and R. Bock, Phys. Rev. Lett. **41**, 625 (1978).
[16]B. Tamain, R. Checkik, H. Fuchs, F. Hanappe, M. Morjean, C. Ngô, J. Péter, M. Dakowski, B. Lucas, C. Mazur, M. Ribrag, and C. Signarbieux, Nucl. Phys. **A330**, 253 (1979).
[17]C. R. Gould, R. Bass, J. V. Czarnecki, V. Hartmann, K. Stelzer, R. Zitzmann, and Y. Eyal, Z. Phys. A **284**, 353 (1978).
[18]T. C. Awes, R. L. Ferguson, R. Novotny, F. E. Obenshain, F. Plasil, S. Pontoppidan, V. Rauch, G. R. Young, and H. Sann, Phys. Rev. Lett. **52**, 251 (1984).
[19]R. Vandenbosch, A. Lazzarini, D. Leach, D.-K. Lock, A. Ray, and A. Seamster, Phys. Rev. Lett. **52**, 1964 (1984).
[20]H. Sohlbach, H. Freiesleben, P. Braun-Munzinger, W. F. W. Schneider, D. Schüll, B. Kohlmeyer, M. Marinescu, and F. Pühlhofer, Phys. Lett. **153B**, 386 (1985); H. Sohlbach, H. Freiesleben, W. F. W. Schneider, D. Schüll, P. Braun-Munzinger, B. Kohlmeyer, M. Marinescu and F. Pühlhofer, Nucl. Phys. **A467**, 349 (1987); H. Sohlbach, H. Freiesleben, W. F. W. Schneider, D. Schüll, B. Kohlmeyer, M. Marinescu, and F. Pühlhofer, Z. Phys. A **328**, 205 (1987).
[21]L. G. Sobotka, G. J. Wozniak, R. J. McDonald, M. A. McMahan, R. J. Charity, L. G. Moretto, Z. H. Liu, F. S. Stephens, R. M. Diamond, and M. A. Deleplanque, Phys. Lett. B **175**, 27 (1986).
[22]J. L. Wile, W. U. Schröder, J. R. Huizenga, and D. Hilscher, Phys. Rev. C **35**, 1608 (1987).
[23]D. R. Benton, H. Breuer, F. Khazaie, K. Kwiatkowski, V. Viola, S. Bradley, A. C. Mignerey, and A. P. Weston-Dawkes, Phys. Rev. C **38**, 1207 (1988); Phys. Lett. B **185**, 326 (1987). D. R. Benton, Ph.D. thesis, University of Maryland, 1986.
[24]B. Schürmann, W. Nörenberg, and M. Simbel, Z. Phys. **286**, 263 (1978).
[25]R. Płaneta, K. Kwiatkowski, S. H. Zhou, V. E. Viola, H. Breuer, M. A. McMahan, W. Kehoe, and A. C. Mignerey, Phys. Rev. C **41**, 942 (1990), the preceding paper.
[26]A. Gavron, Phys. Rev. C **21**, 230 (1980).
[27]W. W. Wilcke, J. R. Birkelund, H. Wollersheim, A. D. Hoover, J. R. Huizenga, W. U. Schröder and L. Tubbs, At. Data Nucl. Data Tables **25**, 529 (1980).
[28]R. Bass, Nucl. Phys. **A231**, 45 (1974).
[29]L. G. Sobotka, C. C. Hsu, G. J. Wozniak, D. J. Morrissey, and L. G. Moretto, Nucl. Phys. **A371**, 510 (1981).
[30]L. G. Moretto, *Proceedings of the International Conference on Nuclear Physics, Florence, 1983* (unpublished).
[31]J. Töke, W. U. Schröder, and J. R. Huizenga, Phys. Rev. C **40**, 1577 (1989).
[32]U. Brosa and S. Grossman, J. Phys. G **10**, 933 (1984); and private communication.
[33]H. Keller, B. Bellwied, K. Lützenkirchen, J. V. Kratz, W. Brüchle, H. Gäggler, K. J. Moody, M. Schädel, and G. Wirth, Z. Phys. A **328**, 255 (1987).
[34]P. J. Siemens, J. P. Bondorf, D. H. E. Gross, and F. Dickman, Phys. Lett. **36B**, 24 (1971).
[35]R. Płaneta, S. H. Zhou, K. Kwiatkowski, W. G. Wilson, V. E. Viola, H. Breuer, D. Benton, F. Khazaie, R. J. McDonald, A. C. Mignerey, A. Weston-Dawkes, R. T. deSouza, J. R. Huizenga, and W. U. Schröder, Phys. Rev. C **38**, 195 (1988).
[36]J. Błocki, R. Płaneta, and K. Grotowski, *Proceedings of the XXIV Zakopane School on Nuclear Physics, 1989,* edited by J. Styczen and Z. Stachura (World Scientific, Singapore, 1990).
[37]D. J. Morrissey and L. G. Moretto, Phys. Rev. C **23**, 1835 (1981).
[38]H. Breuer, N. R. Yoder, A. C. Mignerey, V. E. Viola, K. Kwiatkowski, and K. L. Wolf, Nucl. Instrum. Methods **204**, 419 (1983); Phys. Rev. C **28**, 1080 (1983).
[39]W. J. Swiatecki, Prog. Nucl. Part. Phys. **4**, 383 (1980).
[40]H. Breuer, A. C. Mignerey, V. E. Viola, K. L. Wolf, J. R. Birkelund, D. Hilscher, J. R. Huizenga, W. U. Schröder, and W. W. Wilcke, Phys. Rev. C **28**, 1080 (1983).
[41]H. Stege, H.-J. Keim, H. A. Bösser, B. Kohlmeyer, F. Pühlhofer, and W. F. W. Schneider, Nucl. Phys. **A489**, 146 (1988).